SLAC-PUB-11477

Measurements of radiation near an atomic spectral line from the interaction of a 30 GeV electron beam and a long plasma

P. Catravas, S. Chattopadhyay, E. Esarey, W.P. Leemans

Lawrence Berkeley National Laboratory, University of California, Berkeley, CA 94720

R. Assmann*, F.-J. Decker, M.J. Hogan, R. Iverson, R.H. Siemann, D. Walz, D. Whittum

Stanford Linear Accelerator Center, Stanford University, Stanford CA 94309

**present address: CERN, European Organization for Nuclear Research, Geneva, Switzerland*

B. Blue, C. Clayton, C. Joshi, K.A. Marsh, W.B. Mori, S. Wang

University of California Los Angeles, Los Angeles CA 90095

T. Katsouleas, S. Lee, P. Muggli

University of Southern California, Los Angeles CA 90089

(October 31, 2000)

Abstract

Emissions produced or initiated by a 30 GeV electron beam propagating through a ∼1 m long heat pipe oven containing neutral and partially ionized vapor have been measured near atomic spectral lines in a beam-plasma wakefield experiment. The Cerenkov spatial profile has been studied as a function of oven temperature and pressure, observation wavelength, and ionizing laser intensity and delay. The Cerenkov peak angle is affected by the creation of plasma; estimates of plasma and neutral density have been extracted. Increases in visible background radiation consistent with increased plasma recombination emissions due to dissipation of wakefields were simultaneously measured.

Submitted to Phys.Rev.

Work supported in part by Department of Energy contract DE-AC02-76SF00515

Laser and particle beam driven plasma wakefield accelerators[1-3] are studied as alternatives to conventional RF accelerators due to their potential of providing accelerating gradients that are several orders of magnitude larger. The wakefield amplitude is maximized when the length of the driving pulse L (electron bunchlength or laser pulselength) is on the order of the plasma wavelength, λ_p, where $\lambda_p = 2\pi c/\omega_p$, $\omega_p = \sqrt{N_e e^2/m_e\epsilon_0}$, and N_e is the electron plasma density [1]. For drive beams with a duration τ_b of 0.1 to 1 ps, the corresponding plasma densities are $10^{17} - 10^{15}$ cm^{-3}.

In this Letter, we investigate how radiation produced or initiated by the electron beam near atomic spectral resonances of the medium can provide an opportunity to characterize the plasma and wake properties. Two types of radiation are considered: Cerenkov radiation and recombination light. Cerenkov radiation [4] is produced when the speed of light in the medium, c/n, is less than that of the electrons, u. The index of refraction of the medium, neglecting absorption, can be modelled by

$$n - 1 \sim \sum_{species,s} \frac{N_s e^2 f_{ik}}{2m_e\epsilon_0(\omega_{res}^2 - \omega^2)} - \frac{N_e}{2N_{cr}} \tag{1}$$

where N_s is the species density, f_{ik} is the oscillator strength, ω_{res} is the frequency of the atomic resonance, and N_e/N_{cr} is the ratio of the electron density N_e to the critical density $N_{cr} = \omega^2 m_e\epsilon_0/e^2$ at the observation frequency ω. The index of refraction of the medium contains a strong positive contribution from atomic spectral lines on the long wavelength side of the resonance, which can exceed the negative contribution from plasma, and set the index of refraction well above $\beta = u/c$ for specific regions of the spectrum. Cerenkov radiation is then produced with an intensity distribution that is peaked at the phase matched cone angle, $\gamma^{-2} + \theta_c^2 \sim \theta_c^2 \sim 2(n-1)$ (small angles). Through Eq. (1), the Cerenkov cone angle and wavelength thresholds can in principle provide a measure of changes in N_s and ω_{res}. Cerenkov radiation can thus respond on the timescale of the beam bunchlength, τ_b, to parameters which are important in the plasma wakefield interaction, such as ground state neutral and plasma density, which determine N_s, as well as strong electric and magnetic fields, which can shift ω_{res}. Recombination emissions near atomic spectral lines can result

from ionization and excitation due to collisions between plasma electrons and the medium, decaying on timescales much greater than τ_b, long after the passage of the electron beam first excites the wake. Such spectroscopy is of potential interest for understanding of the dynamics of the wake.

In the E157 plasma wakefield acceleration experiment [3] at the Stanford Linear Accelerator Final Focus Test Beam, a 2 ps (rms) long, 30 GeV electron beam bunch with $2\text{x}10^{10}$ particles in a 30-100 μm spot traverses a Li heat pipe [5] oven (Fig. 1). An ArF Excimer laser operating at 193 nm (UV) partially ionized the Li [6,7]. The UV was incoupled and outcoupled by dielectric coated fused Silica foils, 150 μm thick, separated by 2.5 m. The opposite side of the foil was coated with Al for electron beam spot size monitoring using optical transition radiation (OTR) [8]. Images of the downstream OTR foil and far field (focus at infinity) radiation intensity profiles upstream and downstream were measured with 14 and 16 bit cooled CCD's. The plasma density seen by the electron beam was changed by varying the time between laser and electron beam injection. In this scheme, the electron bunch blows out plasma electrons, producing transverse focussing forces along the bunch (that lead to betatron oscillations in the beam envelope) and longitudinal accelerating forces as the plasma electrons return at the electron bunch tail. The design value of plasma density, $2\text{x}10^{14}$ cm^{-3}, was chosen to optimize both the longitudinal field and the fraction of the tail electrons which can experience acceleration. Measurements described below were taken with two ovens, one of Li column length 1.35 m [7], plugged by He at a partial pressure of 450 mTorr, the other of length 1 m at 200 mTorr [6]. The Li neutral density was typically $\sim 10^{15}$ cm^{-3}.

FIGURES

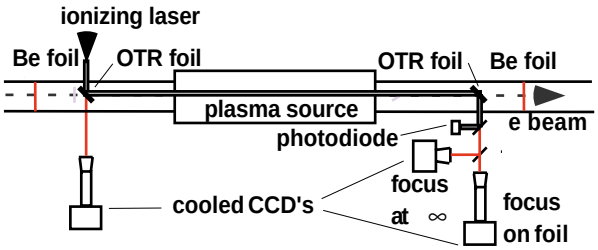

FIG. 1. Experimental setup

Expressions for the spectral flux density and photon levels of Cerenkov radiation can be found in standard texts [4]. The spatial profile was benchmarked with He and Li at various wavelengths. Measurements above 670.8 nm are over 600 nm redshifted from the He ground state atomic resonance of 58.4 nm, and the index of refraction changes little. However, in Li, changes in the observation wavelength of 10's of nm near 670.8 nm, the Li ground state resonance, produce significant changes in the index of refraction. Density measurements in a Helium-filled oven at room temperature at 676.4 nm agreed to within 10% with the density given by the ideal gas law at 100 Torr and 400 Torr. In the heat pipe oven, in which the Li column is confined by two short He plugs, concentric cones corresponding to the Li and He regions were observed (Fig 2a). Far field images recorded from 676.4 nm (1.5 nm BW) to $<$ 670.8 nm are shown in Fig 2b. We observed: i) disappearance of Cerenkov radiation from Li on the short wavelength side of the resonance, where the index of refraction drops below β, ii) increase in cone radius and iii) increase in the cone width as the observation wavelength approaches the spectral line. Dispersive effects dominate the cone radius and width in frame 3 of Fig 2b. The asymmetry of Fig 2b is due to the surface irregularity of a splitting pellicle added to the system. Li Cerenkov cones were compared at 800 nm, 700 nm and 676.4 nm and, despite the increasing proximity to the spectral resonance, yielded estimates of neutral density which agreed within 7%.

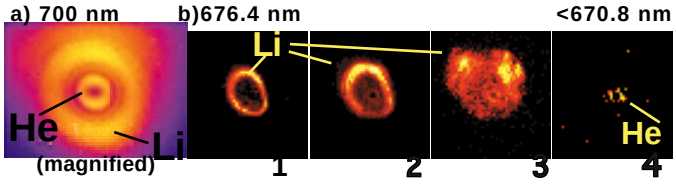

FIG. 2. a) Far field image (537 °C) shows separate cones for the Li and He regions. b) Far field wavelength scan from 676 nm through and below the resonance shows disappearance of Li Cerenkov cone, and trends in cone radius and width. Wavelength decreases from left to right.

The spatial profile of the Cerenkov radiation was recorded at the downstream foil (see Fig. 1) at 676.4 nm, 1.5 nm BW, during oven cool down to study the dependence of Cerenkov cone angle θ_c on oven temperature, T, and pressure. The measured He plug pressure was 270 mTorr for the scan in Fig. 3, giving N_n of 2.6x10^{15} cm^{-3} from pressure balance in "oven mode." At the operating temperature, the neutral density estimated from the Cerenkov cone was 2.1x10^{15} cm^{-3}, in reasonable agreement with pressure balance. The neutral density scaling with T as the Li vapor changes state is $N_n \sim T^{-1} \exp(-\phi/kT)$, where k is the Boltzmann constant. The dependence on T of the neutral densities estimated from θ_c are plotted in Fig. 3 along with known values [9]. Cone peak angles were calibrated using far field measurements and the difference between measured exterior shield temperature and interior oven temperature, left as a fit parameter, was found to be 20°C. The slope of Fig. 3b is relatively insensitive to such a shift in external to internal temperature, and the corresponding heat of vaporization per atom ΔH_v, came within $5-10\%$ of the known value for Li, 1.54 eV [9] both at 676 and 700 nm.

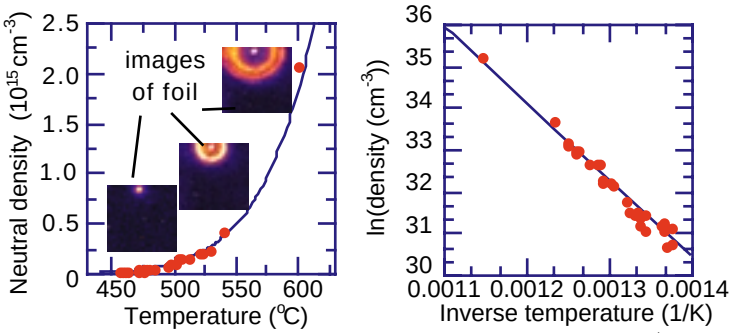

FIG. 3. a) Neutral density estimated from Cerenkov radiation and b) its functional dependence are plotted for an oven cool down. The solid lines are known vaporization curves [9].

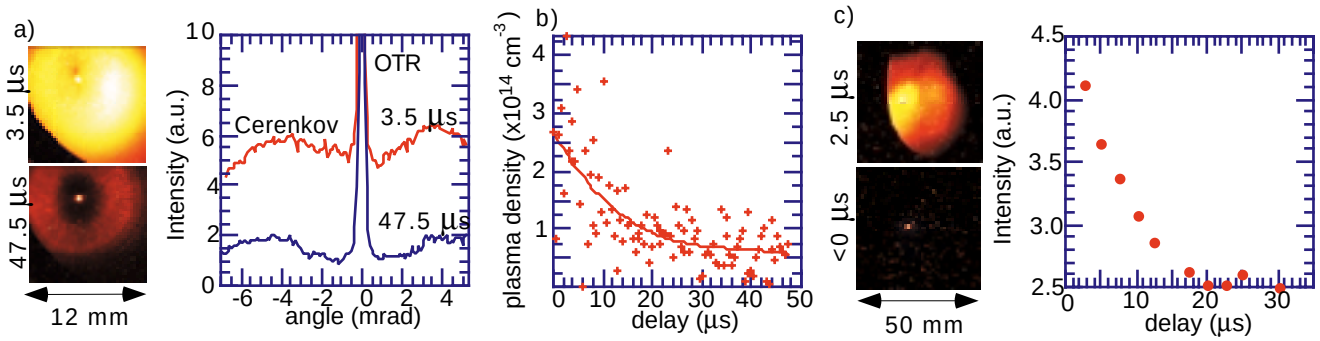

FIG. 4. Downstream foil data are shown for two wavelength ranges: (a-b) 676.4 nm (1.35 m oven) and (c) 505 nm (1 m oven). a) Images at high (3.5 μs delay) and low (47.5 μs) plasma density. Lineouts show inward shift of Cerenkov cone and increase in visible background level. b) Plasma density estimated from inward shift of Cerenkov cone angle vs. delay c) Images at $\Delta t < 0$ and 2.5 μs delay show spatial extent (limited by 2 in. pellicle aperture) of background; total intensity collected into 80 nm BW vs. delay.

The dependence of the Cerenkov spatial profile on plasma production was studied at 676 nm by scanning the relative delay Δt between the electron beam and the ionizing laser by up to 50 μs, (i.e. a few plasma decay times). Two strong effects were observed. First, θ_c shifted inward in the presence of plasma. Second, the Cerenkov cone was riding on a substantial background signal which appeared in the presence of plasma with an intensity dependent on wavelength, on timing delay Δt and on coalignment.

Fig 4a shows the images of a thin foil 1.33 m downstream from the oven center at 676 nm for delays Δt of 3.5 and 47.5 μs, after subtraction of the baseline radiation pattern from the red hot oven wick over a 0.5 s integration time. The central spot in the images is due to optical transition radiation, which was used for transverse profiling of the electron beam. The three constituents of these images (Cerenkov cone, OTR at center and background) were separated by incrementally subtracting images from consecutive time steps, starting from laser off and working toward smaller delays, Δt. Once the slow varying component was quantified and removed, the spatially separate Cerenkov cone peak angle and OTR width were determined. The Cerenkov cone angle systematically decreased with decreasing delay (increasing plasma density). At the same time, the OTR images of the transverse profile of the electron beam showed that the number of betatron oscillations executed by the electron beam along the length of the oven decreased by about one oscillation as the plasma density available immediately after laser fire to decreased to that of 47 μs after laser fire. The electron beam spot size went through minima at delays of 6 and 37 μs. A maximum occurred at 14 μs; another maximum was being approached near 0 delay. Substantial increases in the visible background appeared with decreasing delay with a time constant on the order of the plasma decay time. These observations are analyzed in more detail below.

Plasma density causes inward shifting of the Cerenkov cone. The fractional ionization, (N_i/N_n), where N_i is the ion density, can be quantified from θ_c when the observation wavelength is chosen sufficiently far from resonance that shifts in ω_{res} can be neglected. A baseline measurement without plasma gives initial neutral density. Depletion of the neutral population reduces the cone angle and the ratio to the baseline angle will be proportional to $\sqrt{1 - N_i/N_n}$. The plasma density extracted from the Cerenkov cone radius is shown in Fig 4b. The estimated initial plasma density is 2.6x10^{14} cm^{-3}. The factor of 4 decrease in density in 35 μs is approximately the same as measured previously [7], but the two experiments have different detailed time dependencies.

The plasma density extracted from the Cerenkov cone can be compared with that required to produce the observed number of betatron oscillations in the OTR images of the beam spot size. The relation between plasma density and the betatron wavelength, λ_β, assuming that the plasma ions exert a linear restoring force on the electron beam, is given by $\lambda_\beta = \sqrt{2\gamma}\lambda_p \propto {N_e}^{-1/2}$. Plasma density diagnosis based on measurement of betatron oscillations has been studied experimentally [11,12]. Including the transverse focussing over the plasma column length and adding the short drift space to the OTR foil, the spot size at the foil was calculated as a function of plasma density. Notice that for this analysis, given the plasma density which remained at 47 μs according to Fig. 4b, a spot size minimum at delay greater than 50 μs is expected, implying that the two pinches recorded during the scan were the second and third pinch. The observed betatron oscillations can be explained in the range of initial plasma densities and best-square-fit Li plasma lengths of 1-2x10^{14} cm^{-3} and 1.4-1.0 meter, respectively. The nominal oven length was 1.35 m, so the latter result would imply either that the effective length of the plasma column was shorter (which could result if the ionizing laser was not perfectly collimated or if the oven was not in oven mode when these measurements were made) or that there is roughly 50% disagreement between these two measurements of plasma density.

The Cerenkov cone radius was also studied as a function of the ionizing laser energy near zero delay. The extracted plasma density was linear with UV fluence. The plasma density extracted from Cerenkov radiation (Fig. 4b) is consistent with plasma density estimated from UV absorption assuming a 1x3 mm spot size, 0.72 mJ incident energy at the plasma, and 14% fractional ionization.

The dependence of the background intensity on incident UV fluence and delay at 676 nm was studied. In both cases, the background increased linearly with the plasma density extracted from the Cerenkov cone shift. The timing dependence of the total number of intercepted photons was compared at different wavelengths, 700 nm (40 nm BW, 1% transmission at 670.8 nm), 676.4 nm (1.5 nm BW, 1.7% transmission at 670.8 nm), 632 nm (1 nm BW), and 505 nm (80 nm BW). The background intensity was strong for the 676.4 nm and 505 nm filters, intermittent for the 700 nm filter, but dropped by three orders of magnitude at 632 nm.

The use of a 505 nm filter provided measurement of background radiation without additional contributions either from Li Cerenkov radiation or from recombination radiation near 670.8 nm. The measurements with the 505 nm filter were taken with the 1 m oven [6]. In Fig. 4c, the spatial profiles are compared for negative delay (ebeam arrives before laser) and for 2.5μs delay and total intercepted intensity is plotted against delay, Δt. (Note that this includes a constant contribution from OTR.) The background intensity was steering dependent; the intensity reduced and disappeared as the laser was pivoted upstream from the oven entrance to be out of alignment with the electron beam.

We speculate that additional recombinations due to wake energy dissipation through ionization and excitation of the medium produced the increase in visible background radiation [14], leaking through the tails in the filter spectral response. For design values of $\sim$100 MeV lost per electron in the bulk of a beam with $\sim 10^{10}$ particles, the total stored energy in the wakefield is 3 orders of magnitude greater than that absorbed from the ionizing laser. Recombination light from the UV-ionized plasma only (beam off) was recorded as the interference filter was tilted to pass through to the short wavelength side of the atomic spectral line. Because the integration time of the CCD camera is 0.5 s, much longer than the relative timing scan of 50-100 μs, recombination of plasma ionized by the UV laser cannot explain the delay-dependent effect.

Synchrotron radiation from beam bending and betatron motion could not account for the observed effect because of discrepancies in number of photons and spatial profile characteristics. Synchrotron radiation was considered because a systematic increase in e beam steering with increasing plasma density was observed during the scan of Fig. 4a-b, reaching a displacement of 300 μm at the OTR foil 1.33 m downstream from center of the plasma, corresponding to a bending radius of curvature of $\rho \sim$4.4x10^3 m. The number of photons expected at 676 nm [13] is too low by several orders of magnitude and the spatial characteristics are inconsistent. Radiation from three betatron periods has an on-axis resonant frequency in the X-rays, and will have an increasing intensity with decreasing visible wavelengths. However, the visible background was not present at all wavelengths on the short wavelength side of the resonance.

In this paper, errors are typically a factor of two. Sources of error include background subtraction, filter tilts, non-uniform oven profiles, etc. Another potential contribution is resonant frequency shift due to the Stark or Zeeman effect. Simulations for optimized parameters of the beam-plasma interaction predict electric fields of 100 MeV/m over the bulk of the beam and magnetic fields ranging from 2 T to >15 T at pinches. Self fields from the beam are below 400 MeV/m. The Stark shift for the $2S^{1/2}$ to $2P^{1/2}$ transition of Li is reported in the literature [10] to be 4.062 kHz/(kV/cm)^2; Zeeman shifts are 28 GHz/T. As the observation wavelength approaches resonance, refractive effects due to transverse variation in index of refraction may become important. However, comparison of the ratio of radii of measured Cerenkov cones at 676, 700 and 800 nm indicated that resonant frequency shifts must have been small.

In a future experiment, the error bars on the measured cone shifts can easily be improved by an order of magnitude with additional extinction of the background signal (at the longer wavelengths with respect to resonance) and a larger field of view for precise density diagnosis. A spectrometer, streak spectrometer or FROG should be used to compare radiation characteristics at different wavelengths and times along the bunch. Time resolving the long wavelength Cerenkov cutoff, which is a function of $N_e/2N_{cr}$, can give plasma blowout information. Since the Stark shift is quadratic with field strength, the short wavelength cutoff offers intriguing possibilities to measure large field gradients.

We thank M.S. Zolotorev, B. Shadwick, L. Archambault, M. Dickinson and S. DiMaggio for their contributions. This research was funded by the DOE, Grants DE-AC-03-76SF0098, DE-AC03-76SF00515, DE-AC-03-76SF0098 and DE-FG03-98-DP-00211, and NSF Contract ECS9617089.

REFERENCES

[1] For a review, see E. Esarey et al., IEEE Trans. on Plas. Sci., *24*, p. 252-288 (1996).

[2] J.B. Rosenzweig, Phys.Rev.A, *44*, p 6854 (1991). N. Barov et al., Phys. Rev. Lett., *80*, p. 81 (1998)

[3] M.J. Hogan et al., Phys. Plasmas, *7*, p. 2241 (2000).

[4] W.K.H. Panofsky and M. Phillips, *Classical Electricity and Magnetism*, Addison-Wesley Pub. Co., Inc. (1962).

[5] C.R. Vidal et al., J. Appl. Phys., *40*, p. 3370 (1969).

[6] S. DiMaggio et al., Proc. 1999 Particle Accelerator Conference, New York, p. 3705 (1999).

[7] P. Muggli et al., IEEE Trans. Plas. Sci, *27*, p. 791 (1999).

[8] P. Catravas et al., Proc. 1999 Particle Accelerator Conference, New York, p. 2111 (1999).

[9] AIP Handbook, D.E.Gray, Ed., McGraw Hill, NY (1972).

[10] L.R. Hunter et al., Phys. Rev. A, *44*, p.6140 (1991).

[11] R. Siemann, SLAC Tech Pub. ARDB-221 (2000).

[12] C. Clayton et al., in preparation.

[13] K.J. Kim, AIP Conf. Proc., *184*, p.565-632 (1989).

[14] Max Zolotorev, private communication.